Diffraction of a Shock Wave by a Compression Corner: I. Regular Reflection

Paul Kutler* and V. S. Vijaya Shankar†
NASA Ames Research Center, Moffett Field, Calif.

The unsteady, two-dimensional flowfield resulting from the interaction of a moving planar shock wave with a compression corner is determined using a second-order, discontinuity-fitting, finite-difference approach. The time-dependent Euler equations are transformed to normalize the distance between the body and the peripheral shock and to include the existing self-similar property of the flow. The resulting set of partial differential equations in conservation-law form is then solved in a time-dependent fashion using MacCormack's scheme. The vortical singularity, which lies on the body surface, and the single reflected shock are both treated as discontinuities in the numerical procedure. The results of the numerical simulation are qualitatively very similar to the existing experimental interferograms and yield better flowfield resolution than previous first-order, shock-capturing, numerical solutions.

Introduction

FOR well over a quarter of a century, experimentalists[1-7] and theoreticians[8-21] have been studying the problem of shock wave diffraction, that is, the deflection of a shock wave whose normal path has been impeded by some obstacle. Current interest in this problem has been generated by researchers[22] investigating the nuclear blast fields around aerospace vehicles and around flush-mounted surface structures in an attempt to accumulate a data base for survivability and vulnerability studies. Such parametric information can be used to determine the nonuniform dynamic loading to be applied in structural analysis programs for the design of present-day or future generic aerospace systems.

The interaction of a spherical blast wave with a planar surface results in the complete range of shock reflections; that is, from regular reflection at 0° incidence of the blast wave with the surface (Fig. 1a) to Mach reflection at 90° incidence (Fig. 1b). The determination and understanding of this interaction is of importance not only to the structural engineer interested in the transient blast loading effects but also to the aerodynamicist interested in the mechanics of the flowfield.

The simplest laboratory experiment designed to study the shock diffraction problem consists of a two-dimensional wedge or ramp mounted on the wall of a shock tube (see Fig. 2). Depending on the angle of inclination of the ramp with respect to the shock tube wall θ_r and the strength of the planar incident shock (with Mach number M_s), either regular or Mach reflection occurs. Regardless of the type of reflection process, this shock diffraction problem is self-similar with respect to time since there is no characteristic length associated with the problem.

The self-similar flowfield that results from regular reflection of the incident shock at the surface of the wedge (see Fig. 2a) is not as complicated as that for Mach reflection. The regularly reflected shock is straight up to the sonic circle and then curves to become perpendicular to the shock-tube wall, and between the circle and the shock impingement point the flow is uniform. In the physical plane, the flow follows the shock wave, whereas, in the self-similar plane, the flow moves away from the shock wave and in a direction toward the ramp.

In this problem, there exist two self-similar stagnation points, that is, points at which the self-similar velocity components $\bar{U}=u-x/t$ and $\bar{V}=v-y/t$ are zero; the firstis located at the juncture of the wall and ramp (where the streamlines appear as a saddle point), and the second, termed a vortical singularity, is located at some point along the ramp (where the streamlines appear as a nodal singularity). All streamlines in the self-similar plane converge at the nodal point or vortical singularity, and, therefore, the entropy is multivalued. At the saddle point, the streamlines turn away, and the entropy is regular. The level of entropy on the stagnation streamline and along the ramp up to the vortical singularity is equal to that behind the normal part of the reflected shock, whereas the level of the entropy along the ramp between the vortical singularity and the incident shock impingement point is equal to that behind the straight part of the reflected shock.

From an analysis of the equations governing the flow behavior in the vicinity of conical, self-similar stagnation points,[10,23] it can be shown that the pressure is a local maximum at the saddle point of streamlines, and this point corresponds to a centerpoint of isobars. Similarly it can be shown that the pressure is a local minimum at the nodal point of streamlines, and this point corresponds to a saddle-point of isobars. These features of all inviscid, conical, self-similar flowfields can be observed in the pressure contour plots presented in the Results section of this paper.

A typical Mach reflection case for weak incident shock waves is shown in Fig. 2b. This self-similar flowfield, which will be treated in a later paper,[24] is somewhat complicated by the existence of a triple point at which the incident, reflected,

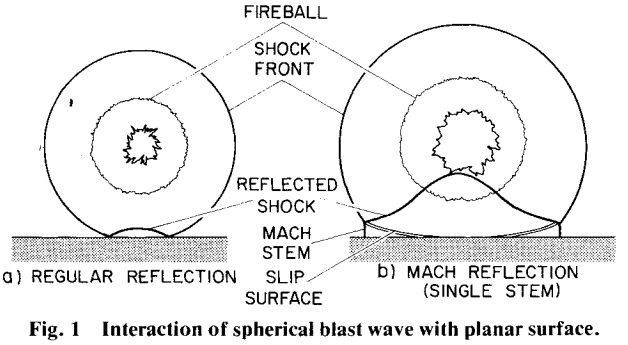

Fig. 1 Interaction of spherical blast wave with planar surface.

Received June 28, 1976; presented as Paper 76-323 at the AIAA 9th Fluid and Plasma Dynamics Conference, San Diego, Calif., July 14-16, 1976; revision received Oct. 20, 1976.

Index categories: Supersonic and Hypersonic Flow; Shock Waves and Detonations; LV/M Aerodynamics.

*Research Scientist, Computational Fluid Dynamics Branch. Associate Fellow AIAA.

†Research Assistant, Iowa State University. Student Member AIAA.

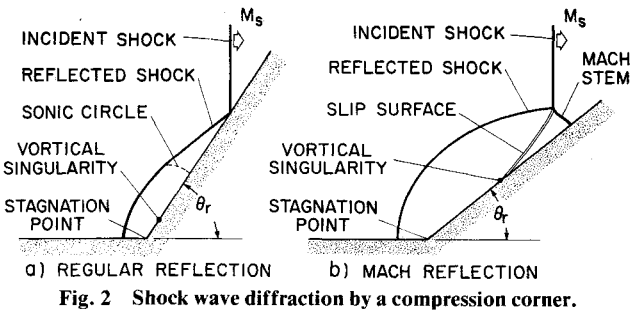

Fig. 2 Shock wave diffraction by a compression corner.

and Mach stem shock waves meet. Emanating from the triple point is a slip surface that intersects the ramp at the vortical singularity. The numerical solution of the Mach reflection problem employs a transformation that normalizes not only the distance between the reflected shock and ramp (as presented here for the regular reflection case), but also the distance between the wall and Mach stem. Thus two separate problem formulations are required and hence two independent computer codes.

In the present paper, the two-dimensional, time-dependent Euler equations that govern these flows are solved with initial conditions that result in regular reflection of the incident shock. The hyperbolic partial differential equations are transformed to include self-similarity and then normalized between the ramp and the reflected shock. The self-similar transformation reduces these equations from an unsteady to an equivalent steady set of mixed elliptic-hyperbolic equations; that is, in the shock layer between the wall and the sonic circle (see Fig. 2a), they are elliptic, whereas above the sonic circle they are hyperbolic. The equations are made totally hyperbolic by reintroducing a time-like or residual term, which should approach zero in the converged solution. The final set of equations is written in strong conservation-law form and then solved using MacCormack's[25] second-order, finite-difference algorithm.

Unlike previous numerical solutions,[11,12,14,21] both the vortical singularity and the peripheral shock wave are treated as sharp discontinuities, thus resulting in a more accurate description of the inviscid flowfield. To impose the surface tangency condition at the wall and along the ramp, a number of boundary condition procedures are tried, including that of Kentzer,[26] in an attempt to employ the simplest yet most accurate one. The resulting numerical solutions are compared with available experimental data and existing first-order, shock-capturing numerical solutions.

Governing Equations

A Cartesian coordinate system is used in the problem formulation, the origin of which is located at the intersection of the wall and the ramp. The x axis is aligned with the wall, and the y axis is normal to the wall and in the direction of the ramp (see Fig. 3a). Under the assumption of an inviscid, non-heat-conducting, ideal gas, the fluid dynamic equations in strong conservation-law form[27,28] for the independent variable transformation $\tau=t$, $\eta=\eta(t,x,y)$, and $\xi=\xi(t,x,y)$ are

$$(U/\delta)_\tau+[(U\eta_t+E\eta_x+F\eta_y)/\delta]_\eta + [(U\xi_t+E\xi_x+F\xi_y)/\delta]_\xi=0 \tag{1}$$

where

$$U=\begin{bmatrix}\rho\\ \rho u\\ \rho v\\ e\end{bmatrix} \quad E=\begin{bmatrix}\rho u\\ p+\rho u^2\\ \rho uv\\ (e+p)u\end{bmatrix} \quad F=\begin{bmatrix}\rho v\\ \rho uv\\ p+\rho v^2\\ (e+p)v\end{bmatrix}$$

and $\delta=\eta_x\xi_y-\eta_y\xi_x$.

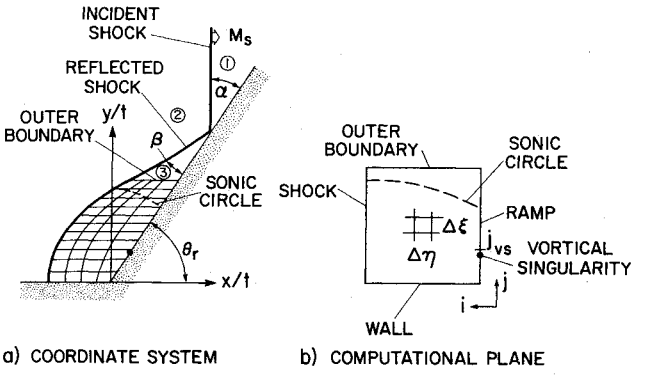

Fig. 3 Coordinate system and computational plane.

In the conservative variables of Eq. (1), p represents the pressure; ρ, the density; u and v, the velocity components in the x and y directions; and e, the total energy per unit volume. The pressure, density, and velocity are related to the energy for an ideal gas by the following equation

$$e=p/(\gamma-1)+\rho(u^2+v^2)/2 \tag{2}$$

The following functions are used for τ, η, and ξ, which include the self-similarity of the problem and a normalization of the distance between the ramp and the reflected shock:

$$\tau=t$$

$$\eta=[x-x_b(y)]/[x_s(t,y)-x_b(y)]$$

$$\xi=y/t \tag{3}$$

where $x_b(y)=y\cot\theta_r$ represents the equation of the ramp, and where $x_s(t,y)$ represents the equation of the shock. The partial derivatives required by Eq. (1) are

$$\eta_t=-\eta x_{s_t}/(x_s-x_b) \qquad \xi_t=-\xi/\tau$$

$$\eta_x=1/(x_s-x_b) \qquad \xi_x=0$$

$$\eta_y=-[x_{b_y}-\eta(x_{s_y}-x_{b_y})]/(x_s-x_b) \qquad \xi_y=1/\tau \tag{4}$$

The transformed, time-dependent Euler equations, which are hyperbolic with respect to τ, are solved using a time asymptotic approach. Because of the self-similar transformation, the $(U/\delta)_\tau$ term in Eq. (1) approaches zero as τ increases, thus establishing a convergence criterion.

Boundary and Initial Conditions

The transformation given by Eq. (3) results in the computational plane shown in Fig. 3b. It is bounded by the reflected shock wave and outer boundary, both of which are permeable surfaces, and by the wall and ramp surfaces, both of which are impermeable surfaces. The boundary-condition procedures applied at each of these surfaces and the initial conditions are discussed following.

Reflected Shock Wave

The position and shape of the reflected shock wave are determined at each step of the time-asymptotic integration procedure. The variables x_s, x_{s_y}, and x_{s_t} that appear in the conservative variables of Eq. (1) along the flow variables at the shock can be determined by employing an unsteady variation of Thomas' "pressure approach"[29,30] for propagating shock waves. In this approach, it is only necessary to know the pressure behind the shock to alter its position for the next time level. The required pressure is obtained by using the normal field point predictor-corrector algorithm at the shock but with one-sided differences away

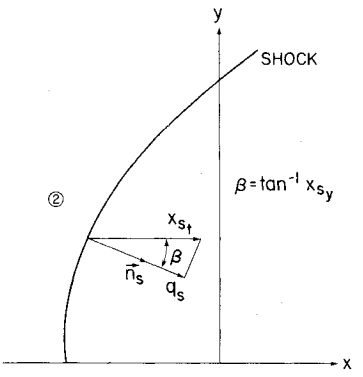

Fig. 4 Shock propagation in an unsteady flow.

from the shock or in the η direction. The shock speed (see Fig. 4) and remaining flow variables are given by the following equations, which include the Rankine-Hugoniot relations

$$x_{s_t} = q_s/\cos\beta \tag{5a}$$

where

$$\beta = \tan^{-1} x_{s_y}$$

$$q_s = \tilde{u}_x - a_2 M_x$$

$$M_x = \left\{ \frac{1}{2\gamma}\left[\frac{p_s}{p_2}(\gamma+1) + (\gamma-1) \right] \right\}^{1/2}$$

$$\tilde{u}_x = |u_2|/\sqrt{1+x_{s_y}^2}$$

$$a_2 = (\gamma p_2/\rho_2)^{1/2}$$

$$x_{s_y} = x_{s_\xi}\xi_y$$

and

$$\rho_s = \rho_2[(\gamma+1)M_x^2]/[(\gamma-1)M_x^2+2] \tag{5b}$$

$$u_s = u_2 + (\tilde{u}_y - \tilde{u}_x)/\sqrt{1+x_{s_y}^2} \tag{5c}$$

$$v_s = -[(\tilde{u}_y - \tilde{u}_x)x_{s_y}/\sqrt{1+x_{s_y}^2} \tag{5d}$$

$$\tilde{u}_y = M_y a_s + q_s$$

$$M_y = \left[\frac{(\gamma-1)M_x^2+2}{2\gamma M_x^2 - (\gamma-1)} \right]^{1/2}$$

$$a_s = (\gamma p_s/\rho_s)^{1/2}$$

$$e_s = p_s/(\gamma-1) + \rho_s(u_s^2+v_s^2)/2 \tag{5e}$$

The quantity x_{s_ξ} in Eq. (5a) is determined numerically using a second-order central difference formula. The subscript 2 in Eq. (5) refers to the uniform flow region 2 of Figs. 2a and 4. The flow variables in region 2 are given in terms of the known flow quantities of region 1 and the incident shock Mach number by the following equations for a moving shock

$$p_2 = p_1[2\gamma M_s^2 - (\gamma-1)]/(\gamma+1) \tag{6a}$$

$$\rho_2 = \rho_1\left(\frac{\gamma+1}{\gamma-1}\frac{p_2}{p_1} + 1 \right)\Big/\left(\frac{\gamma+1}{\gamma-1} + \frac{p_2}{p_1} \right) \tag{6b}$$

$$u_2 = M_s\left[1 - \frac{(\gamma-1)M_s^2+2}{(\gamma+1)M_s^2} \right]\left(\frac{\gamma p_1}{\rho_1} \right)^{1/2} \tag{6c}$$

The actual propagation of the shock wave in the numerical procedure is accomplished by using a second-order Euler predictor/modified Euler corrector

$$x_s^{(1)} = x_s^n + x_{s_\tau}^n \Delta\tau \quad \text{predictor} \tag{7a}$$

$$x_s^{n+1} = x_s^n + \tfrac{1}{2}[x_{s_\tau}^n + x_{s_\tau}^{(1)}]\Delta\tau \quad \text{corrector} \tag{7b}$$

where $x_{s_\tau} = x_{s_t} + x_{s_y} y_\tau$, $\Delta\tau$ is the integration step size, and x_{s_t} (see Fig. 4) is given by Eq. (5a).

The above equations are used as follows: Initially at time step n all flows variables at the shock are known, including the shock shape and speed. The pressure behind the shock is predicted using the first step of MacCormack's scheme. The shock wave is then moved using Eq. (7a), and the predicted position permits the shock derivative x_{s_ξ} to be computed. The shock speed, density, velocity components, and energy are then calculated from Eq. (5). The same procedure is used in the corrector step except that the second step of MacCormack's scheme is used and Eq. (7b) is used to correct the shock position.

Impermeable Boundaries

The impermeable boundaries in the shock-diffraction problem consist of the wall surface and the ramp surface. Each of these boundaries is aligned with a constant coordinate line as a result of the self-similar, normalizing transformation. Because of this alignment and the fact that the flow must be tangent to these boundaries, the only variable required at the body to advance the field points according to Eq. (1) is the pressure. However, determination of the remaining flow variables and the position of the vortical singularity on the ramp surface is essential in computing this pressure. Discussed below are two different boundary condition procedures that were tested for satisfying the tangency condition and determining the flow variables along the wall and ramp surfaces.

In the first, a simple Euler predictor/modified Euler corrector with one-sided ξ derivatives at the wall and η derivatives at the ramp for Eq. (1) is used. The tangency condition itself, that is, $v=0$ at the wall and $v=u\tan\theta_r$ along the ramp, is imposed after the corrector step. Having determined the velocity components from this procedure, the self-similar velocities $\bar{U}=u-x/t$ and $\bar{V}=v-y/t$ are usedto locate the vortical singularity by noting at what position along the ramp they are identically zero. Knowing this location, the appropriate entropy levels are assigned to the surface grid points. As mentioned in the Introduction, the level of entropy at node points along the wall and on the ramp up to the vortical singularity is equal to that behind the normal part of the reflected shock, whereas the level of entropy at node

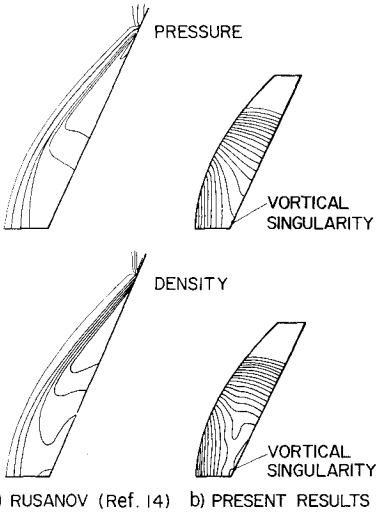

Fig. 5 Comparison of numerically generated pressure contour plots; $M_s = 1.89, \theta_r = 65°$.

points between the vortical singularity and the incident shock impingement point is equal to that behind the straight part of the reflected shock. The corresponding body density is obtained from the following expression by using the pressure computed by the one-sided finite-difference scheme

$$\rho = (p/s)^{1/\gamma} \tag{8}$$

where s is the appropriate entropy level. The total energy e is then recomputed using Eq. (2).

The second boundary condition procedure tested was that of Kentzer.[26] It is based on a method of characteristics approach in combination with one-sided finite differences. The equations for the characteristics and the compatibility relations along those characteristics are derived both in the $\eta - \tau$ and $\xi - \tau$ planes; the purpose is to derive an expression for p_τ valid at the body points that can be integrated to obtain the surface pressure.

For the wall, the compatibility relation corresponding to the down-running characteristics in the $\xi - \tau$ plane is combined with the surface tangency condition in differential form ($v_\tau = 0$) to yield the following

$$p_\tau = -c\xi_y(\rho c v_\xi - p_\xi) - (\bar{u}p_\eta + \rho c^2 \eta_x u_\eta - c\eta_y p_\eta) \tag{9a}$$

$$u_\tau = -u_\eta \bar{u} - p_\eta \eta_x/\rho \tag{9b}$$

Similarly, for the ramp surface, the compatibility relation corresponding to the down-running characteristic in the $\eta - \tau$ plane is combined with the flow tangency condition in differential form ($v_\tau = u_\tau \tan\theta_r$) to yield

$$p_\tau = -A_0 p_\eta + \frac{\rho c \eta_x}{(\eta_x^2 + \eta_y^2)^{1/2}} A_1 + \frac{\rho c \eta_y}{(\eta_x^2 + \eta_y^2)^{1/2}} A_2 - A_3 \tag{10a}$$

$$u_\tau = -u_\xi \bar{v} - p_\eta \eta_x/\rho \tag{10b}$$

where

$$c = (\gamma p/\rho)^{1/2}$$

$$\bar{u} = \eta_t + u\eta_x + v\eta_y$$

$$\bar{v} = \xi_t + u\xi_x + v\xi_y$$

$$A_0 = -c(\eta_x^2 + \eta_y^2)^{1/2}$$

$$A_1 = -u_\xi \bar{v} - p_\eta \eta_x/\rho + A_0 u_\eta$$

$$A_2 = (-u_\xi \bar{v} - p_\eta \eta_x/\rho)\tan\theta_r + A_0 v_\eta$$

$$A_3 = \bar{v}p_\xi + \rho c^2 \xi_y v_\xi - \frac{\rho c \eta_x}{(\eta_x^2 + \eta_y^2)^{1/2}} \bar{v} u_\xi - \frac{\rho c \eta_y}{(\eta_x^2 + \eta_y^2)^{1/2}} (\xi_y p_\xi/\rho + \bar{v} v_\xi)$$

By combining the compatibility relation with the tangency condition in differential form, the disadvantages of the true method of characteristics (the iteration and interpolations required to get data at specific points on a characteristic) are eliminated.

Equations (9) and (10) are integrated in the normal predictor-corrector fashion with the ξ and η derivatives replaced by one-sided finite differences to obtain the pressure and u velocity at the body points. Having the u velocity component, the v velocity component is computed from the surface tangency condition. The self-similar velocities, position of the vortical singularity, and body density are computed in the same way as described for the previous boundary condition procedure.

Using the self-similar property of the flowfield in conjunction with the surface tangency condition, it can be shown from the normal momentum equation that $\partial p/\partial n$ (where n is the direction normal to each surface) is zero at the wall and ramp surfaces. Neither Kentzer's scheme nor the Euler predictor/modified Euler corrector method satisfy this condition exactly because of the approximate one-sided, finite-differences involved. Therefore, after the converged solution is obtained using either of the above boundary condition procedures, the pressure at the body is recomputed after the corrector step to satisfy $\partial p/\partial n = 0$. A comparison of the different boundary-condition schemes is presented in the Results section of this paper.

Outer Boundary

The outer boundary (see Fig. 3) must be positioned beyond the sonic circle whose equation is

$$(u_3 - x_{sc}/t)^2 + (v_3 - y_{sc}/t)^2 = a_3^2 \tag{11}$$

where u_3, v_3, and a_3 are known in the uniform flow region 3. This results in the outer boundary being a supersonic inflow boundary[29] and allows the flow conditions along it to be specified initially and held fixed during the entire integration procedure.

Initial Conditions and Step Size

To initialize the flowfield at time $\tau = 1$, given the incident shock Mach number M_s and ramp angle θ_r, the pressure and density in region 1 (see Fig. 3a) are first set equal to unity. The flow conditions in region 2, which are used as the upstream conditions for the reflected shock, can now be calculated from Eq. (6) for a moving shock. The position and slope of the reflected shock along with the uniform flow conditions in region 3 are then determined from the equivalent steady, regular shock reflection equations. These conditions determine the position of the sonic circle at $\tau = 1$ [see Eq. (11)] and thus its intersection with the reflected shock.

Between this intersection point and the wall or plane of symmetry, a cubic is used to approximate the shock shape. Knowing the shock shape and assuming a self-similar flow, that is, $x_{s_\tau} = x_s/\tau$, the flow variables behind the shock wave can be computed.

To initialize the flow variables between the ramp and the shock, the conditions at the stagnation point are first computed based on the flow behind the normal part of the shock. Along the ramp between the stagnation point and the sonic circle, a parabolic approximation of the flow variables is assumed. The field points are then initialized by a linear interpolation of the flow variables at the ramp and reflected shock.

The integration stepsize $\Delta\tau$ must be specified to initiate the calculation. Using a one-dimensional, amplification matrix, stability analysis[31] of MacCormack's scheme, a governing step size for $\Delta\tau$ relative to the η and ξ directions can be found

$$\Delta\tau_\eta = CN\,\Delta\eta / |\eta_t + u\eta_x + v\eta_y \pm c(\eta_x^2 + \eta_y^2)^{1/2}| \tag{12a}$$

$$\Delta\tau_\xi = CN\,\Delta\xi / |\xi_t + u\xi_x + v\xi_y \pm c(\xi_x^2 + \xi_y^2)^{1/2}| \tag{12b}$$

where CN is the Courant number and is usually set to 0.9. For the calculation to be stable, the minimum of the stepsizes in Eq. (12) is used

$$\Delta\tau = \min(\Delta\tau_\eta, \Delta\tau_\xi) \tag{13}$$

Results

The computational grid for a typical shock-diffraction case consisted of 11 points in the η direction and 27 points in the ξ

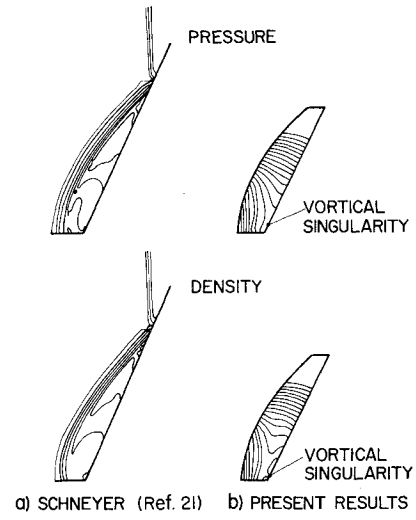

Fig. 6 Comparison of numerically generated pressure contour plots; $M_s = 2, \theta_r = 63.41°$.

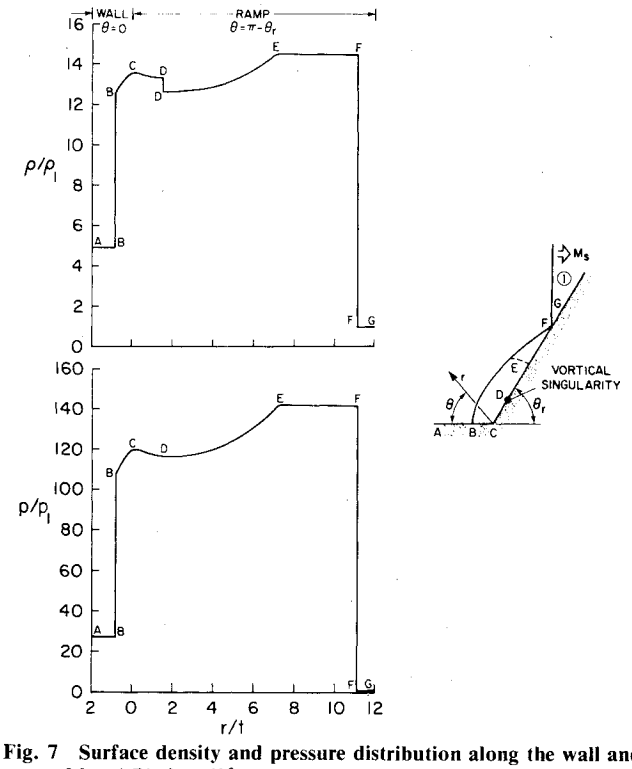

Fig. 7 Surface density and pressure distribution along the wall and ramp; $M_s = 4.71, \theta_r = 60°$.

direction. An average of 300 iterations was required to obtain a converged solution and these consumed approximately 15 min computer time on an IBM 360/67.

Numerical results in the form of pressure and density contour plots are qualitatively compared with the first-order shock-capturing results of Rusanov[14] (Fig. 5) and Schneyer[21] (Fig. 6). Rusanov's solution was obtained using Godunov's method for an incident shock Mach number of 1.89 impinging on a 65° ramp. Most of the contours that appear in Fig. 5a lie within the captured shock wave, and very few describe the flowfield between the ramp and reflected shock in comparison with the contours of Fig. 5b.

In studying the Mach reflection phenomenon, Schneyer[21] used a two-dimensional, Eulerian, hydrodynamic code to obtain the regular reflection result shown in Fig. 6a. The incident shock Mach number was 2.0 and the ramp angle was

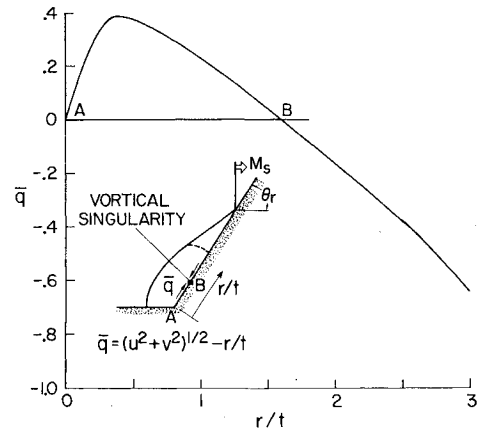

Fig. 8 Self-similar surface velocity distribution; $M_s = 4.71, \theta_r = 60°$.

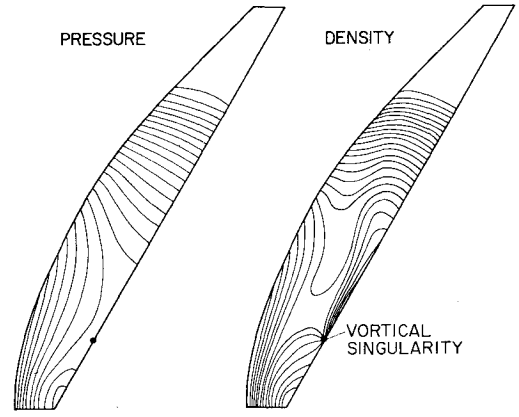

Fig. 9 Comparison of ramp surface pressure distributions for different boundary condition procedures; $M_s = 4.71, \theta_r = 60°$.

63.41°. His result exhibits the same qualitative behavior as does Rusanov's. The present result for the same case is shown in Fig. 6b. The results of both Schneyer and Rusanov fail to reveal the presence of the vortical singularity.

Law[5] performed a series of experiments on the shock-diffraction problem for various gases using a Mach-Zehnder interferometer. In so doing, he tested a Mach 4.71 incident shock striking a 60° ramp in oxygen; the result was regular reflection. This case in addition to others at the same incident shock Mach number but for different ramp angles were obtained numerically to demonstrate the flowfield behavior in the regular reflection regime. The results are presented in Figs. 7-13.

The density and pressure distributions along the wall and ramp are shown in Fig. 7. At the stagnation point (point C of Fig. 7), the density and pressure reach a local maximum, while at the vortical singularity (point D of Fig. 7), the pressure is continuous and at a local minimum, and the density is discontinuous. A partial plot (see Fig. 8) of the self-similar velocity along the ramp reveals the two self-similar stagnation points at A (corresponding to the wall-ramp intersection point) and B (corresponding to the vortical singularity).

In Fig. 9, results from the different body boundary condition procedures are compared. Both the Euler predictor/modified Euler corrector and Kentzer's scheme yield very nearly the same result. The oscillations near the stagnation point are a result of the one-sided, finite-differences used in these schemes. Imposing $\partial p/\partial n = 0$ seems to yield a much better solution without any oscillations in the flow variables near the stagnation point.

Pressure and density contour plots of the computational region are shown in Fig. 10. The center point of isobars near the wall-ramp intersection point, and the saddle point of

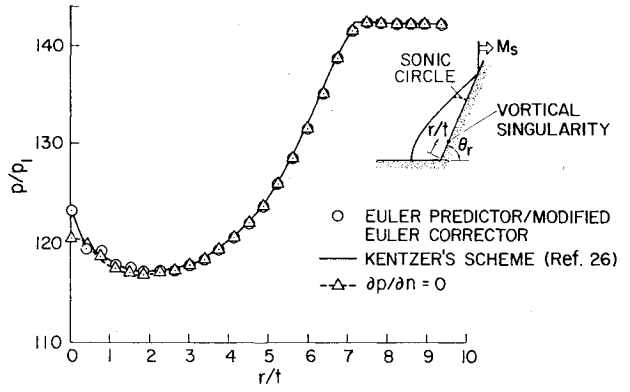

Fig. 10 Pressure and density contour plots; $M_s = 4.71$, $\theta_r = 60°$.

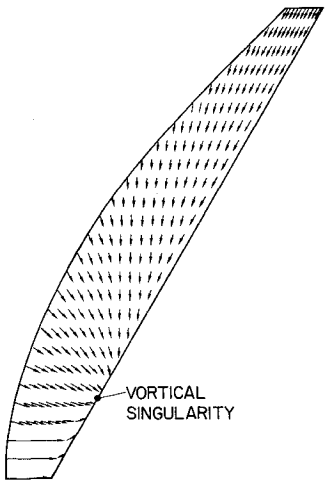

Fig. 11 Self-similar velocity directional plot; $M_s = 4.71$, $\theta_r = 60°$.

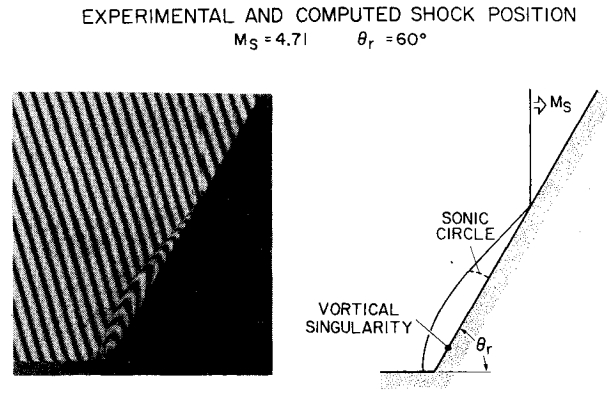

Fig. 12 Comparison of experimental and computed shock positions; $M_s = 4.71$, $\theta_r = 60°$.

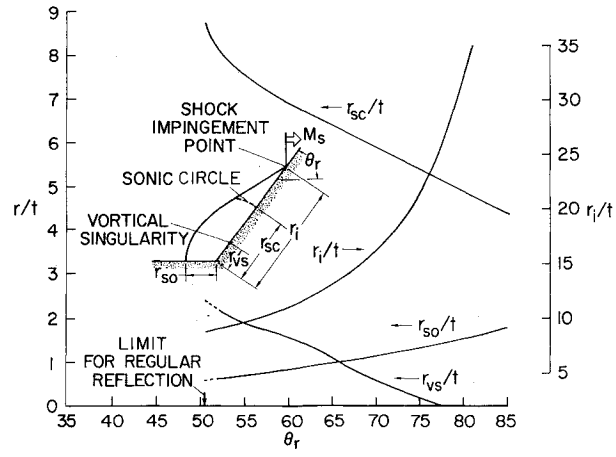

Fig. 13 Variation of geometrical variables with ramp angle; $M_s = 4.71$.

isobars near the vortical singularity (for which moving away from the vortical singularity the pressure increases along the ramp and decreases perpendicular to the ramp) can be clearly observed in Fig. 10. In the density contour plot, the convergence of various isopycnics at the vortical singularity can be observed. The behavior of the flow near the stagnation points in this unsteady two-dimensional self-similar problem exhibits the same behavior as the steady, self-similar, three-dimensional flow about an external axial corner.[32]

The self-similar streamline pattern can be visualized by observing the velocity vector directional plot of the computational plane shown in Fig. 11. Notice that all the streamlines converge at the vortical singularity.

A comparison of the interferogram obtained by Law[5] with the numerically computed shock shape is shown in Fig. 12. If an overlay of the two results were made by matching shock impingement points, the experimental shock location would fall inside the numerical solution. The reason for the discrepancy is probably twofold. First, the viscous effects (the majority of which can be observed near the wall-ramp intersection point) might have the effect of decreasing the ramp angle as a result of the boundary-layer growth with distance from the shock impingement point. The reduced ramp angle in turn results in a smaller shock standoff distance. Second, the computed solution assumes flow of an ideal gas ($\gamma = 1.4$). Thus effects on the internal energy such as molecular, vibrational exictation are not taken into account. It is known[33] that flows of a "real gas" cause shock waves to lie closer to the body than comparable flows of an "ideal gas."

The effect of varying the ramp angle for a given incident shock Mach number of 4.71 on the shock standoff distance (r_{so}), position of the vortical singularity (r_{vs}), location of the sonic circle (r_{sc}), and shock impingement point (r_i) are shown in Fig. 13. The standoff distance exhibits almost a linear variation with ramp angle between the limit for regular reflection and the last case computed of $\theta_r = 85°$. The vortical singularity moves toward the wall with increasing ramp angle and actually attaches itself to the wall for values of θ_r greater than 77°. The location of the sonic circle along the ramp, and the shock impingement point are identical at the limit for regular reflection. As θ_r increases, the sonic circle moves toward the wall while the impingement point moves away from the wall.

Conclusions

The simple procedure developed in this paper for computing the shock-diffraction problem for regular reflection is capable of accurately predicting the inviscid flowfield with its single peripheral shock wave and vortical singularity. The solution in the neighborhood of the self-similar stagnation points exhibits the properties predicted by a simple analysis of the gas-dynamic equations with regards to the behavior of the streamlines, isobars, and isopycnics. The present numerical results are a considerable improvement over the early first-order numerical solutions and compare favorably with existing experimental data.

Structural designers interested in the dynamic loading effects of blast-induced forces sometimes seek only the peak pressures that occur at the surface of a configuration. Such pressures for regular reflection of the incident shock occur directly behind the reflected shock, as shown in Fig. 8, and are, therefore, easily obtained from the procedure outlined in the initial condition section of this paper. However, the designer interested in the frequency response of the system to the induced nonlinear forces requires the complete flowfield for his analysis.

References

[1]Smith, L. G., "Photographic Investigation of the Reflection of Plane Shocks in Air," Office of Scientific Research and Development, Rept. 4943, Washington, D.C., April 1945, pp. 47-67.

[2] Weynants, R. R., "An Experimental Investigation of Shock-Wave Diffraction Over Compression and Expansion Corners," University of Toronto, Institute of Aerospace Studies, Toronto, Canada, UTIAS TN No. 126, April 1968.

[3]Gvozdeva, L. G., Bashenova, T. V., Predvoditeleva, O. A., and Fokeev, V. P., "Mach Reflection of Shock Waves in Real Gases," *Astronautica Acta*, Vol. 14, Jan. 1969, pp. 503-508.

[4]Gvozdeva, L. G., Bazhenova, T. V., Predvoditeleva, O. A., and Fokeev, V. P., "Pressure and Temperature at the Wedge Surface for Mach Reflection of Strong Shock Waves," *Astronautica Acta*, Vol. 15, Jan. 1970, pp. 503-510.

[5]Law, C. K., "Diffraction of Strong Shock Waves by a Compressive Corner," University of Toronto, Institute of Aerospace Studies, Toronto, Canada, UTIAS TN No. 150, July 1970.

[6]Bertrand, B. P., "Measurement of Pressure in Mach Reflection of Strong Shock Waves in a Shock Tube," Ballistic Research Labs, Aberdeen Proving Ground, Md., Memorandum Rept. 2196, June 1972.

[7]Bazhenova, T. V., Gvozdeva, L. G., Komarov, V. S., and Sukhov, B. G., "Diffraction of Strong Shock Waves by Convex Corners," *Izvestiya Akademii Nauk SSSR. Mekhanika Zhidkostii Gaza*, No. 4, July-Aug. 1973, pp. 122-134.

[8]Courant, R. and Friedrichs, K. O., *Supersonic Flow and Shock Waves*, Interscience Publishers Inc., New York, 1948, pp. 334-338.

[9]Bleakney, W. and Taub, A. H., "Interaction of Shock Waves," *Reviews of Modern Physics*, Vol. 21, Oct. 1949, pp. 584-605.

[10]Ludloff, H. F. and Friedman, M. B., "Aerodynamics of Blasts-Diffraction of Blast Around Finite Corners," *Journal of the Aeronautical Sciences*, Vol. 22, Jan. 1955, pp. 27-34.

[11]Ludloff, H. F. and Friedman, M. B., "Difference Solution of Shock Diffraction Problem," *Journal of the Aeronautical Sciences*, Vol. 22, Feb. 1955, pp. 139-140.

[12]Belotserkovskii, O. M. and Chushkin, P. I., "The Numerical Solution of Problems in Gas Dynamics," *Basic Developments in Fluid Dynamics*, edited by Maurice Holt, Academic Press, New York, 1965, pp. 22-27.

[13]Pack, D. C., "The Reflexion and Diffraction of Shock Waves," *Journal of Fluid Mechanics*, Vol. 18, April 1964, pp. 549-570.

[14]Rusanov, V. V., "Calculation of the Interaction of Non-Stationary Shock Waves and Obstructions," *Journal of Numerical Analysis and Mathematical Physics*, Vol. 1, April 1961, pp. 267-279.

[15]Henderson, L. V., "The Refraction of a Plane Shock Wave at a Gas Interface," *Journal of Fluid Mechanics*, Vol. 26, Pt. 3, Nov. 1966, pp. 607-637.

[16]Whitham, G. B., "A New Approach to Problems of Shock Dynamics: Part I, Two-Dimensional Problems," *Journal of Fluid Mechanics*, Vol. 2, Pt. 2, March 1966, pp. 145-171.

[17]Harlow, F. H. and Amsden, A. A., "Fluid Dynamics," Los Alamos Scientific Laboratory Rept., Los Alamos, N. Mex., LA-4700, June 1971, pp. 43-57.

[18]Wilkins, M. L., "Calculation of Surface and Ground Waves from Above-Ground and Underground Explosions," *Astronautica Acta*, Vol. 17, March 1972, pp. 399-404.

[19]Zumwalt, G. W., "Weak Wave Reflections at Near 90° Angle of Incidence," *Journal of Applied Mechanics*, Dec. 1974, pp. 1142-1143.

[20]Zhigalko, Y. F., "Approximate Locally-Nonlinear Solution of the Problem on Interaction Between a Shock Wave and Rigid Wall," *Fluid Mechanics—Soviet Research*, Vol. 4, March-April, 1975, pp. 81-91.

[21]Schneyer, G. P., "Numerical Simulation of Regular and Mach Reflections," *The Physics of Fluids*, Vol. 18, Sept. 1975, pp. 1119-1124.

[22]Carpenter, H. J. and Brode, H. L., "Height of Burst Blast at High Overpressure," Paper No. H3 presented at the 4th International Symposium on Military Applications of Blast Simulations, Southend-on-Sea, England, Sept. 9-12, 1974.

[23]Bakker, P. G. and Bannink, W. J., "Conical Stagnation Points in the Supersonic Flow Around Slender Circular Cones at Incidence," Delft University of Technology, Delft (The Netherlands), Dept. of Aeronautical Engineering Rept. VTH-184, Nov. 1974.

[24]Shankar, V. S. V., Kutler, P., and Anderson, D. A., "Diffraction of a Shock Wave by a Compression Corner, Part II—Single Mach Reflection," AIAA Paper 77-89, Los Angeles, Calif., 1977.

[25]MacCormack, R. W., "The Effect of Viscosity in Hypervelocity Impact Cratering," AIAA Paper 69-354, Cincinnati, Ohio, 1969.

[26]Kentzer, C. P., "Discretization of Boundary Conditions on Moving Discontinuities," *Lecture Notes in Physics*, No. 8, Springer-Verlag, New York, Sept. 1970, pp. 108-113.

[27]Vinokur, M., "Conservation Equations of Gasdynamics in Curvilinear Coordinate Systems," *Journal of Computational Physics*, Vol. 14, Feb. 1974, pp. 105-125.

[28]Viviand, H., "Conservative Forms of Gas Dynamic Equations," *LaRecherche Aerospatiale*, Vol. 1, Jan.-Feb. 1974, pp. 65-68.

[29]Thomas, P. D., Vinokur, M., Bastianon, R., and Conti, R. J., "Numerical Solution for the Three-Dimensional Inviscid Supersonic Flow of a Blunt Delta Body," *AIAA Journal*, Vol. 10, July 1974, pp. 887-894.

[30]Kutler, P., "Computation of Three-Dimensional, Inviscid Supersonic Flows," *Lecture Notes in Physics*, Springer-Verlag, No. 41, Progress in Numerical Fluid Dynamics, edited by H. J. Wirz, 1975, pp. 287-374.

[31]Richtmyer, R. D. and Morton, J. W., *Difference Methods for Initial-Value Problems*, Wiley, New York, 1967, pp. 302-303.

[32]Kutler, P. and Shankar, V., "Computation of the Inviscid Supersonic Flow over an External Axial Corner," *Proceedings of the 1976 Heat Transfer and Fluid Mechanics Institute*, University of California, Davis, Calif., June 21-23, 1976.

[33]Kutler, P., Reinhardt, W. A., and Warming, R. F., "Multishocked, Three-Dimensional Supersonic Flowfields with Real Gas Effects," *AIAA Journal*, Vol. 11, May 1973, pp. 657-644.